Adaptive Zero Velocity Update Based on Velocity Classification for Pedestrian Tracking

Rui Zhang, Hai Yang, Fabian Höflinger, and Leonhard M. Reindl, *Senior Member, IEEE*

***Abstract*— Due to the drift of low-cost micro-electro-mechanical systems sensors and recursive computation, pedestrian tracking based on foot-mounted inertial sensors suffers from accumulative velocity and position errors. The well-known approach named zero velocity update (ZUPT) is able to minimize such errors by resetting the velocity to zero when the foot does not move with respect to ground. This time duration is called the still phase of a stride and can be detected by comparing the actual sensor data with a pre-defined threshold. However, when the velocity increases or decreases, the fixed threshold may be too small or too big for the correct detection of the still phase. Based on our previous study, this paper presents a novel adaptive ZUPT approach using an additional chest-attached accelerometer for consistent removal of accumulative errors even if the velocity changes. The information extracted from the chest acceleration is used to update corresponding threshold for the still-phase detection, and, hence, to determine error-free velocity and position information. The experimental results show that the accurate tracking trajectory can still be successfully obtained even if the velocity changes rapidly during the experiment.**

***Index Terms*— Zero velocity update (ZUPT), inertial measurement unit (IMU), movement classification, tracking, localization.**

I. Introduction

WITH the fast development of Micro- Electro- Mechanical Systems (MEMS) technology, nowadays MEMS inertial sensors based Dead Reckoning (DR) plays a big role for market of personal localization indoors or outdoors. Instead of utilizing pre-installed network infrastructure, DR only requires sensors to be carried or worn by the person being tracked to add an object's small movements to build its trajectory from a given starting point, making it particularly attractive for localization in unprepared environments [1].

However, low-cost MEMS inertial sensors suffer from the sensor drift and normally require the assistance from other absolute localization systems such as GPS [2]. If no reference is available for the correction of position or velocity information, the accumulative errors of position and velocity will grow with time boundlessly. Ojeda and Borenstein reported that these accumulative errors could be removed by detecting the still-phase of each step [3], [4], during which the foot does not move in respect to the ground, using proper threshold on the condition that the inertial sensors were mounted on the foot to track every detail of the foot's movement. This method is called Zero velocity UPdaTe (ZUPT). Since then this idea has been successfully implemented in several studies [5]–[11], [12].

The performance of ZUPT method highly relies on the accuracy of the still-phase detection. For walking-like movement, the threshold is usually pre-defined empirically. Some literatures reported that a threshold value close to 50 deg/s is a proper choice for movement at normal walking pace [7], [13], [14]. However, when the speed becomes higher, the threshold needs to be updated, since the durations of the still-phase can not be detected using the same threshold value. Foxlin suggested enlarging the step detection threshold when experiencing high-speed movement [5], but no further details were given. Even if the correct threshold value for detecting high-speed movement can be determined, how to switch the threshold values between movements at different speeds is still a problem. ZUPT algorithm must be informed to change the threshold values when the speed of movement starts to change.

We came up with an idea to use an additional tri-axis accelerometer to classify walking-like movements at different speeds and to determine the proper thresholds, in order to consistently detect the correct still-phase [14]. The movement is distinguished by applying wavelet transform to the chest acceleration data according to [15]–[20]. Being not computation-friendly, this real-time approach requires lots of computational power and can not be handled easily by normal ARM processor. Besides, the relation between ZUPT thresholds and chest acceleration for movement distinguishing was found empirically without the knowledge of actual speed of movement. Based on our previous work, this paper reports a easy way to extract the useful information for speed differentiation from chest acceleration and uses a treadmill to determine the thresholds corresponding to different velocities. Thus the relation between the chest acceleration and thresholds is much more precise.

The remainder of this paper is structured as follows: In section II the conventional ZUPT method is presented. In section III the problem statement for current ZUPT method is given. In section IV our adaptive ZUPT method is derived. The experimental result and numerical study are reported in section V. Discussion and conclusion are given in section VI.

II. Zero Velocity Update

According to [4], in the whole phases of a stride during normal walking ΔT, point A on the bottom of the sole is in contact with the ground for a short period of time, called

Manuscript received November 28, 2016; revised January 26, 2017; accepted January 27, 2017. Date of publication February 8, 2017; date of current version March 8, 2017. The associate editor coordinating the review of this paper and approving it for publication was Dr. Arindam Basu.

The authors are with the Department of Microsystems Engineering, University of Freiburg, 79110 Freiburg, Germany (e-mail: rui.zhang@imtek.uni-freiburg.de).

Digital Object Identifier 10.1109/JSEN.2017.2665678

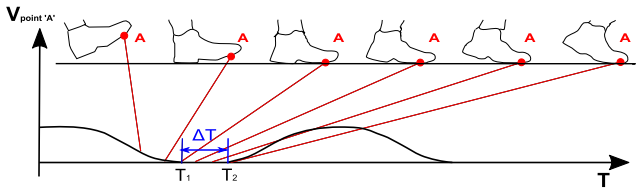

Fig. 1. Key phases in a stride. Adapted from [3, Fig. 2]. The front bottom part of foot A is not moving relative to the ground from T_1 till T_2.

still-phase, as shown in Fig. 1. During this time, 'A' is not moving relative to the ground and the velocity of 'A' is zero. Therefore, the obtained value of velocity by applying navigation equations is expected to be zero during this time as well as acceleration. If the value is not zero, then the difference between zero and the momentary value is assumed to be the accumulated errors during the step interval. As a result, the velocity error should be reset when zero condition is detected. In this way the accumulated errors from the accelerometer output could be effectively removed. This method is called "Zero velocity UPdaTe" (ZUPT), which is firstly introduced by Ojeda and Borenstein [3], [4], and then widespreadly used by most inertial sensor based personal navigation systems. Notice that for normal walking ΔT is about 0.3-0.6 seconds [3], [5], and it changes according to the walking speed.

The performance of the ZUPT based solution highly relies on the detection accuracy of the still-phase. Experimentally the best indication for ΔT could be obtained by observing the outputs of the tri-axis gyroscope. If the norm value of the angular rate vector $\|\boldsymbol{\omega}_k^B\|$ is smaller than pre-defined threshold δ_{ZUPT}, the velocities should be reset.

$$\begin{cases} \|\boldsymbol{\omega}_k^B\| < \delta_{\text{ZUPT}}, & \text{still-phase} \\ \text{otherwise}, & \text{swing-phase} \end{cases} \tag{1}$$

$\|\boldsymbol{\omega}_k^B\|$ is calculated as

$$\left\|\boldsymbol{\omega}_k^B\right\| = \sqrt{(\omega_{x,k}^B)^2 + (\omega_{y,k}^B)^2 + (\omega_{z,k}^B)^2}, \tag{2}$$

where $\boldsymbol{\omega}_k^B = [\omega_{x,k}^B, \omega_{y,k}^B, \omega_{z,k}^B]^T$ stands for the angular rate vector at sampling step k. The superscript B denotes that the vector is in the sensor body coordinate.

The still-phase detection result is depicted in Fig. 2. $C_{\text{still-phase}}$ is the indicator for the still-phase detection, which is defined as

$$C_{\text{still-phase}} = \begin{cases} 1, & \text{still-phase} \\ 0, & \text{swing-phase} \end{cases} \tag{3}$$

The benefit of ZUPT method is depicted in Fig. 3, which shows that the velocity will increase unboundedly if ZUPT method is not applied.

III. Problem Statement

For low-speed walking-like movement the still-phase lasts correspondingly longer and can be detected by comparative smaller threshold noted as $\delta_{\text{ZUPT,1}}$ as shown in Fig. 4. However, when the speed becomes higher, the still-phase will be shorter. Thus, $\delta_{\text{ZUPT,1}}$ can not detect every

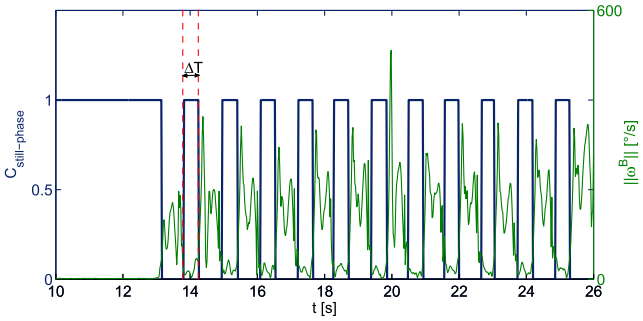

Fig. 2. Result of the still-phase detection using $\delta_{\text{ZUPT}} = \hat{\text{A}}^\circ$ deg/s. ΔT stands for the time duration of the still-phase.

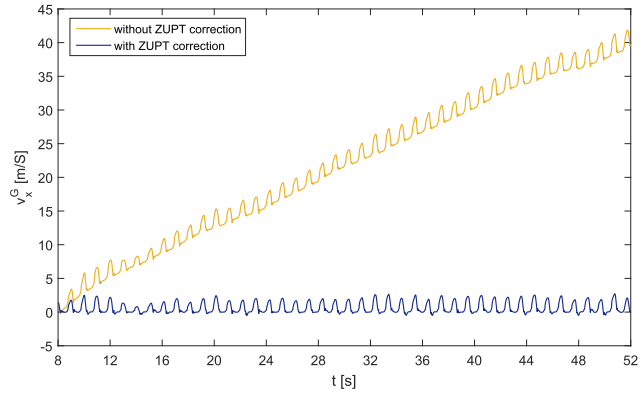

Fig. 3. Comparison of the velocities with and without ZUPT correction. Walking starts from 15 s. The light color signal refers to the velocity values integrated directly from acceleration, and the dark color signal refers to the velocity value being free of accumulative error.

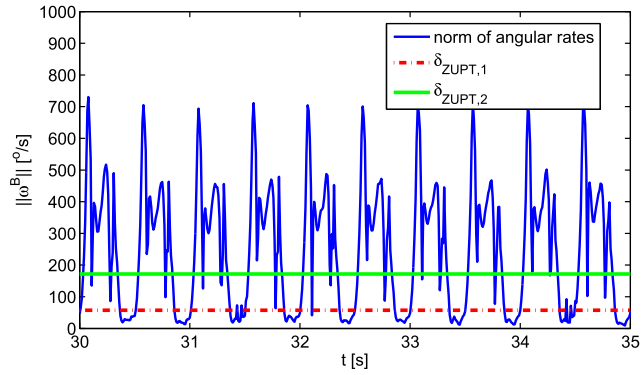

Fig. 4. Still-phase Detection at speed of walking. Both $\delta_{\text{ZUPT,1}}$ (dash line) and $\delta_{\text{ZUPT,2}}$ (continues line) are able to detect each step. The detected still-phase using $\delta_{\text{ZUPT,1}}$ is shorter than the one using $\delta_{\text{ZUPT,2}}$.

point of the still-phase or even the complete still-phase especially when the sampling rate is low, as shown in Fig. 5. Thereby, less foot steps and still-phases are detected and the accumulative errors during the misdetected still-phases can not be removed, which results in a large position error. However, it does not mean that the threshold can be enlarged boundlessly. If threshold is too large, e.g. $\delta_{\text{ZUPT,2}}$ in Fig. 4, the velocity might also be reset during the swing-phase, resulting in less position update of each step after integration. Therefore, it is necessary to develop an ZUPT

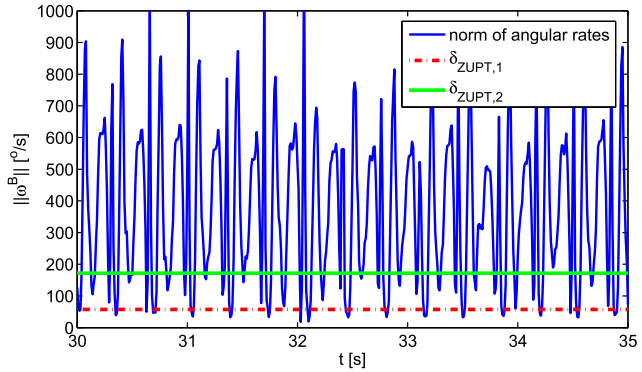

Fig. 5. Still-phase Detection at speed of running. $\delta_{\mathrm{ZUPT},2}$ (continues line) can detect each still-phase. $\delta_{\mathrm{ZUPT},1}$ (dash line) is too small to detect shorter still-phase.

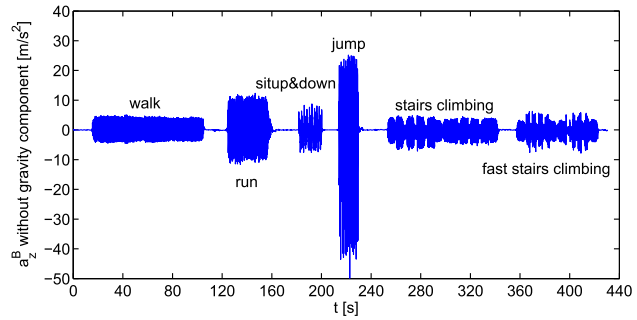

Fig. 6. The plot of gravity-free accelerations of x-axis generated by different activities including walk, run, sit up and down, jump and stairs climbing. Adapted from [15, Fig. 3].

algorithm which can adapt the threshold value for the still-phase detection according to the speed of the movement.

IV. Derivation of Adaptive Zero Velocity Update Algorithm

By attach acceleration sensor on the center of mass of human body, different human activities deliver different accelerations as shown in Fig. 6 [15], [19]. As can be seen that the stronger and more intense the movement is, the larger the variation of acceleration's magnitude is. Therefore, it is possible to recognize and classify the movements at different speeds by analyzing the maximum acceleration change during one foot step.

Instead of extracting the detail and approximation components from the acceleration data using wavelet transform to obtain the characteristic of the movement, as presented in [15]–[20], an easier and more computation-friendly approach is reported in this study. Define maximum acceleration change vector within foot step K as $\mathbf{a}^B_{\mathrm{S},K} = [a^B_{\mathrm{S},x,K}, a^B_{\mathrm{S},y,K}, a^B_{\mathrm{S},z,K}]^T$, which is computed as

$$a^B_{\mathrm{S},x,K} = \left| a^B_{x,K}|_{\max} - a^B_{x,K}|_{\min} \right|, \tag{4}$$

$$a^B_{\mathrm{S},y,K} = \left| a^B_{y,K}|_{\max} - a^B_{y,K}|_{\min} \right|, \tag{5}$$

$$a^B_{\mathrm{S},z,K} = \left| a^B_{z,K}|_{\max} - a^B_{z,K}|_{\min} \right|, \tag{6}$$

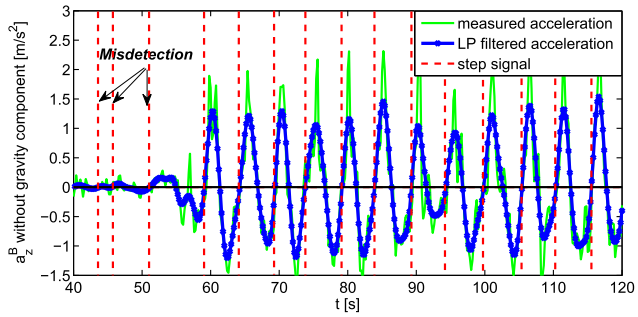

Fig. 7. Step detection using positive-going zero crossing method. Dark and light colored sine-like waves stand for the acceleration data after and before low-pass filtering. The vertical dash lines indicate the time stamps of detected steps. The acceleration signal being analyzed does not contain gravity component.

TABLE I
Sensor Measurement Range and Bandwidth of IMU Module

	angular rate	acceleration	magnetic field
full scale	±1200 [°/s]	±50 [m/s^2]	±750 [mGauss]
bandwidth	40 [Hz]	30 [Hz]	10 [Hz]

where $a^B_{z,K}|_{\max}$ and $a^B_{z,K}|_{\min}$ are the maximum and minimum values of the a^B_z within foot step K. $\mathbf{a}^B = [a^B_x, a^B_y, a^B_z]^T$ stands for the tri-axis acceleration in sensor body coordinate B.

Each step is detected by applying step boundaries to acceleration signals. According to [21] step boundaries are defined by the positive-going zero crossings of a low-pass (LP) filtered version of vertical acceleration signal as shown in Fig. 7. Positive-going zero crossing means that the signal is smaller than zero at last time step and larger than zero at the following time step.

Fig. 7 shows that misdetection does happen when using positive-going zero crossing method. Even a small vibration at the beginning will generate a step signal. However, misdetection is not an issue in this study, since the position information is propagated by strap down integration instead of the summation of constant step length as used in [21].

As can be seen in Fig. 6, a^B_z is definitely a indicator for different movements. However, a^B_z is mainly corresponding to the vertical force (pointing to the ground), which is related to the forward speed, but not able to describe the forward movement comprehensively. Therefore, a^B_x, which is mainly corresponding to the forward force, should be also analyzed to improve the speed differentiation.

A experiment using a treadmill has been carried out for distinguishing different speeds based on a^B_z and a^B_x. The treadmill was set to nine different speeds and its corresponding sub-experiments are: walking at 5 km/h and 7 km/h, running at 6 km/h, 8 km/h, 10 km/h, 12 km/h, 14 km/h, 16 km/h, and 18 km/h. Each running sub-experiments lasts 80 s. 10 s for speeding up and down respectively, 40 s for running at constant speed, and 30 s for rest between sub-experiments. IMU module used in this experiment consists of tri-axis accelerometer, tri-axis gyroscope and tri-axis magnetometer [22]. The measurement range of each sensor is given in Table. I. 2 IMU modules are mounted on the person who walks and runs on

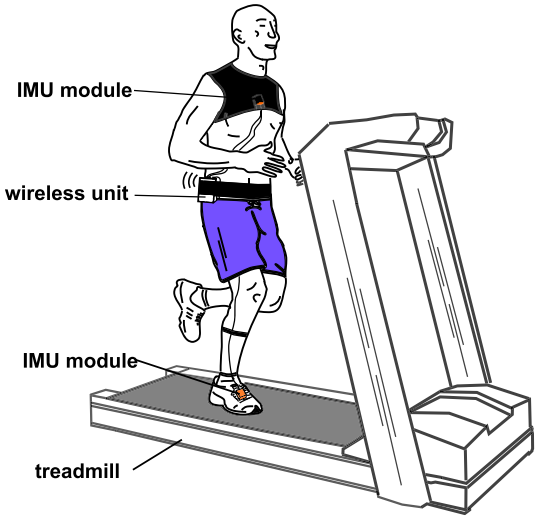

Fig. 8. Experiment setup. Two IMU modules are marked as orange rectangles. Wireless unit transmits the sensor data to the PC for data processing.

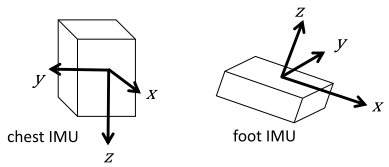

Fig. 9. The orientations of chest- and foot-attached IMU.

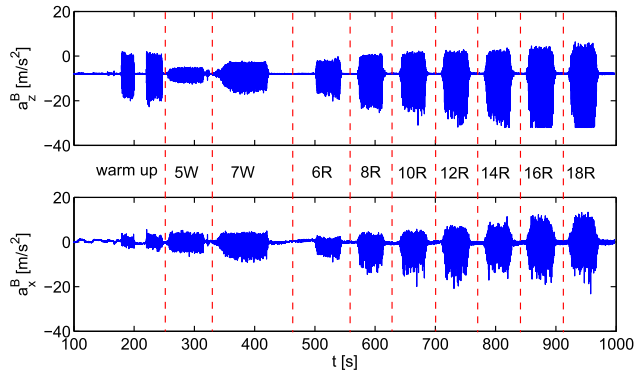

Fig. 10. Accelerations due to the vertical force a_z^B and forward force a_x^B at different speeds.

the treadmill as shown in Fig. 8. The IMU module attached on the chest is for collecting a_x^B and a_z^B. The orientations of both IMU modules are shown in Fig. 9. The IMU module mounted on the foot is used to obtain the velocities and distances of walking/running using ZUPT method, which will be compared with the known references.

The accelerations due to the vertical and forward forces are shown in Fig. 10. For abbreviation, walking at 5 km/h is notated as 5W, and running at 6 km/h is notated as 6R.

The maximum acceleration changes due to the vertical and forward forces of each step are shown in Fig. 11. It can be seen that walking at 7 km/h and running at 6 km/h can not be differentiated by analyzing $a_{S,z}^B$, which might be due to the fact that both movements produce similar vertical forces. However,

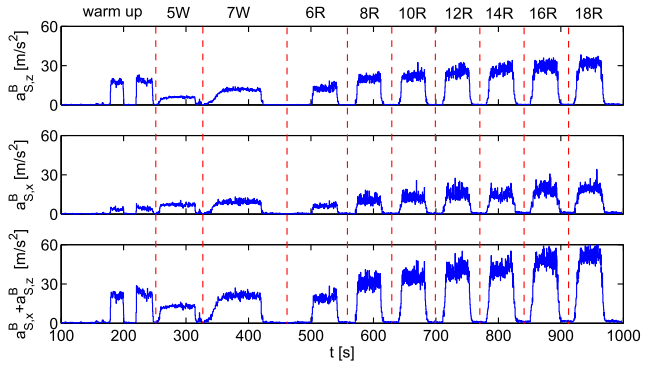

Fig. 11. The maximum acceleration change of each foot step due to the vertical force (above), forward force (middle) and the sum of both forces (bottom) at different speeds.

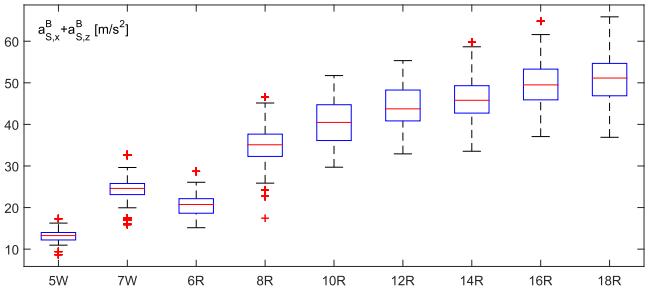

Fig. 12. Average values of $a_{S,z}^B + a_{S,x}^B$ at different speeds depicted as boxplot.

there is an explicit difference shown in $a_{S,x}^B$. But at the same time, the difference of maximum acceleration changes between walking at 5 km/h and running at 6 km/h is more explicit in vertical force instead of forward force, which might be due to the different kinematic movements of human body when walking and running. Therefore, combination of $a_{S,z}^B$ and $a_{S,x}^B$ gives better resolution of speed differentiation, as shown in the third row of Fig. 11.

In order to find the relation between the maximum acceleration changes and corresponding ZUPT thresholds, the average values of $a_{S,z}^B + a_{S,x}^B$ at different speeds is computed and depicted in Fig. 12.

Since the speed and the distance of walking/running of each sub-experiment are known, the correct ZUPT threshold of each sub-experiment can be determined if the exact values can be reproduced after applying ZUPT method and navigation algorithm. The navigation algorithm flow is given briefly as follows: firstly, the orientation is determined by fusing the information from different sensors. Secondly, the gravity component is removed from acceleration data using coordinate transformation. At last, the velocity and position are obtained by taking integrals of gravity-free acceleration data. The algorithm detail can be found in [12]. For all the sub-experiments the still-phases at its corresponding speed can be detected using the threshold values as given in Table. II and shown in Fig. 13.

The relation between $a_{S,z}^B + a_{S,x}^B$ and its corresponding threshold can be obtained by applying an Adaptive

TABLE II
THRESHOLD RANGE FOR THE STILL-PHASE DETECTION AT DIFFERENT SPEEDS

unit	5W	6R	7W	8R	10R	12R	14R	16R	18R
[°/s]	45-90	45-90	55-95	75-95	95-105	135-145	175-195	245-275	250-305

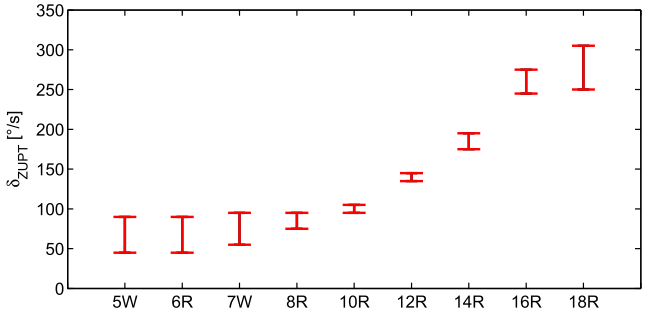

Fig. 13. Corresponding ZUPT threshold ranges at different speeds.

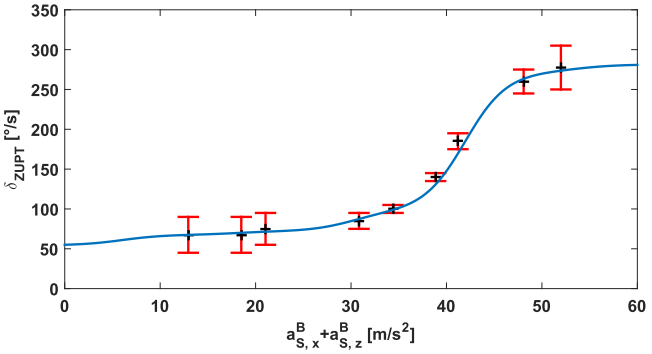

Fig. 14. The relation between the average values of $a^B_{S,z} + a^B_{S,x}$ and its corresponding thresholds for ZUPT still-phase detection interpreted as a hyperbolic tangent curve by using ANFIS.

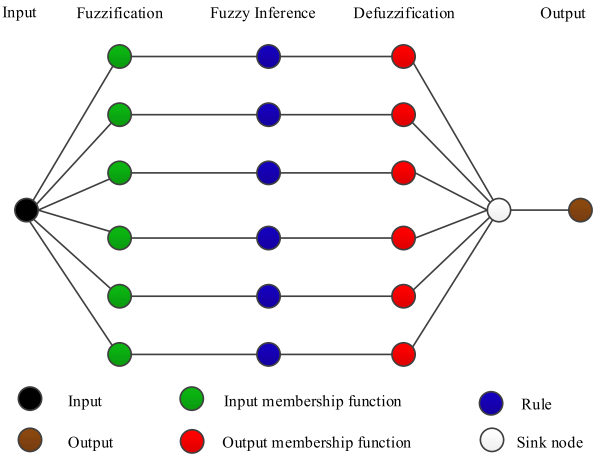

Fig. 15. Model of adaptive neuro-fuzzy inference system.

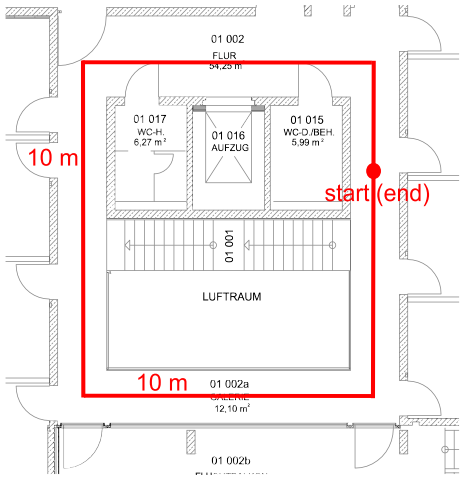

Fig. 16. Building plainmap and trajectory of experiment.

Neuro-Fuzzy Inference System (ANFIS) using Takagi Sugno model. The result is depicted in Fig. 14.

ANFIS is the process of formulating the mapping empirically from a given input to an output using fuzzy logic. The mapping then provides a basis from which decisions can be made, or patterns discerned. ANFIS is mostly used for the system whose control model is too difficult to be mathematically modeled but whose control rules are known. The model of this ANFIS is shown in Fig. 15. 6 membership functions are selected in this case, because the dynamic characteristic of the whole system has limited variation range according to Fig. 13. More membership functions will increase the computational consumption.

The curve, shown in Fig. 14, is very similar to the result based on purely empirical experiments as reported in [14].

V. EXPERIMENTS AND NUMERICAL STUDY

A experiment was carried out to validate proposed adaptive ZUPT algorithm and evaluate its performance. During the experiment a person with two IMU modules firstly walked and then ran along the same rectangular path with a total length of 40 m as shown in Fig. 16.

One IMU module is attached on the chest to differentiate the movements at different speeds and to determine the corresponding ZUPT thresholds for the still-phase detection. The other IMU module is mounted on the foot to apply the proposed navigation algorithm given in [12] using the obtained ZUPT thresholds. The experiment is divided into two phases: walking and running. If the resulted trajectory in running phase is close to the one in walking phase, the adaptive ZUPT algorithm is able to detect the correct still-phase even if the speed is changing. Notice that although the phases are called walking and running phases, the speeds of both phases do not always remain constant. Since in both phases, there are time slots for speed increasing and decreasing. During walking phase, the speed increases from zero to walking speed and then decreases to zero. During running phase, the speed increases firstly from zero to walking speed, and then to running speed. Afterward, the speed decreases to zero again. The proposed ZUPT method must be able to follow the speed change and adaptively provide the corresponding threshold. The sampling rate for data acquisition of IMU modules is set as 50 Hz.

The accelerations in forward and downward directions read from chest-attached IMU module are shown in Fig. 17. It

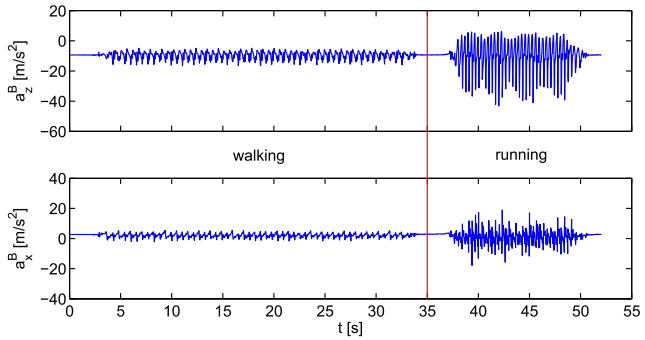

Fig. 17. Forward and downward accelerations of coordinate B a_x^B and a_z^B during walking and running.

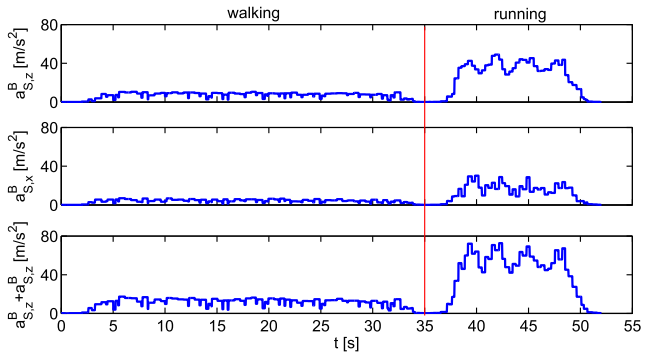

Fig. 18. The maximum acceleration change due to the vertical force (above), forward force (middle) and the sum of both forces (bottom) during walking and running.

can be seen clearly that the acceleration range of running is bigger than the one of walking. The variation of acceleration during running phase is also larger than the one during walking phase. The forward and vertical forces becomes smaller when running around the corner than running straight ahead, since on the corner the speed is firstly reduced and then increased. By using equation (4) and (6), the resulted maximum acceleration changes due to the vertical force, forward force and their sum during walking and running phases are depicted in Fig. 18.

Put $a_{S,z}^B + a_{S,x}^B$ as the input of the ANFIS given in Fig. 14 yields the corresponding ZUPT threshold for the still-phase detection, which is shown in Fig. 19. It can be seen clearly that the threshold remains around $50^o/s$ during walking phase and then climbs up rapidly during running phase. The maximum value of threshold reaches about $250^o/s$.

By using the resulted thresholds, all the still-phases during both walking and running phases can be successfully detected as depicted in Fig. 20. It can be seen that the still-phase duration in walking phase is much longer than in running phase, since the time duration of contact between foot and ground is much shorter when running.

By applying the correct still-phase to the navigation algorithm, even the accumulative acceleration error during running phase can be efficiently removed. The corrected velocities in both phases are plotted in Fig. 21, which shows that the outlines of the velocities in both phases are similar, since the

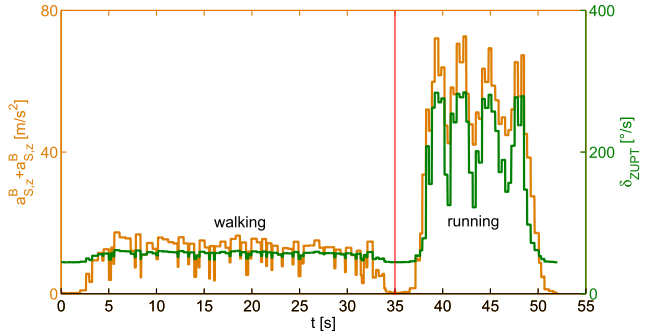

Fig. 19. $a_{S,z}^B + a_{S,x}^B$ v.s. the corresponding threshold for ZUPT still-phase detection.

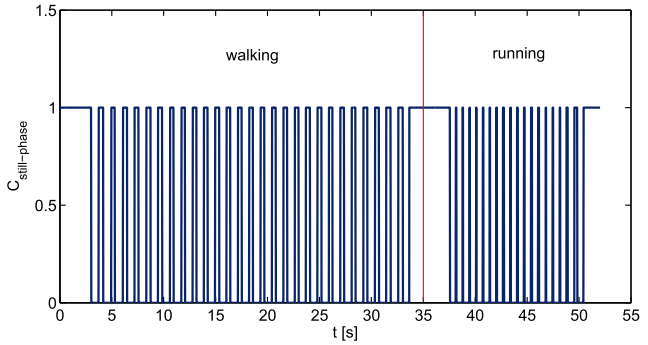

Fig. 20. The still-phase detection result during walking and running phases using adaptive ZUPT method.

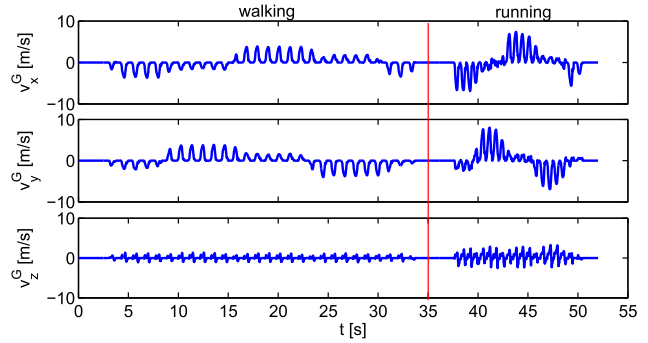

Fig. 21. The resulted velocities during walking and running using adaptive ZUPT method.

person moved along the same rectangular path in both phases. However, in order to cover the same distance in shorter time duration, the velocity magnitude during running phase is larger than the one during walking phase.

Fig. 22 and 23 show the resulted trajectories during both walking and running phases depicted in a 2 dimensional plain plot and a height plot. It can be seen that the trajectories of both phases are similar but there are still some position differences between them. The maximum position error in plain plot reaches about 1 m. Besides, the start and end points can not overlap during running phase. The distance between 2 points is about 1 m. The maximum height error during running phase is about 2.5 m, which is at least 1.5 m larger than the one during walking phase.

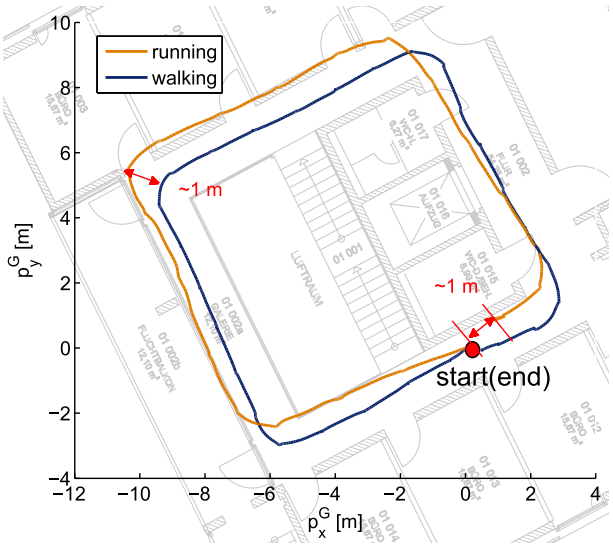

Fig. 22. Comparison of 2D trajectories during walking and running using adaptive ZUPT method.

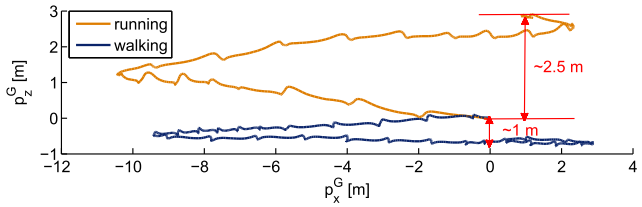

Fig. 23. Comparison of position change in height during walking and running using adaptive ZUPT method.

The larger error shown during running phase might be due to the following reasons. The first reason is the limited sampling rate. When the speed is higher, the same sampling rate might not be sufficient to capture the detail of the movement, which later on affects the still-phase detection. In this case, false-alarm has happened during the still-phase detection and velocity during the swing-phase has been also compressed. The second reason is the imprecise model to link the still-phase detection threshold and the average value of $a^B_{\mathrm{S},z} + a^B_{\mathrm{S},x}$ as shown in Fig. 14. Although the model is based on walking/running at nine different speeds covering from 5 km/h to 18 km/h, the resolution of speed climbing is fairly big, which is either 1 km/h or 2 km/h. Therefore the accuracy of resulted model which is just based on nine points curve fitting might not be sufficient. Besides, there are a range of threshold values which are able to reproduce the known speed or distance as given in Table. II. Therefore, there are many possibilities for implementing the curve fitting. Perhaps the chosen fitted curve is not the most accurate one. The last factor is actually the sensor's measurement range given in Table. I. When the speed becomes higher, the actual sensor data might be very close to or even beyond the sensor's maximum measurement range and the error of the sensed data will grows accordingly. Hence, the correctness of orientation and velocity becomes doubtful.

Table. III and IV show the maximum 2D position and height errors for tracking of 10 pedestrians with changing velocity

TABLE III
MAXIMUM 2D POSITION ERROR FOR DIFFERENT PEDESTRIANS

max.err. [m]	60-75 kg	76-90 kg
age 20-30	1.37	1.16
age 31-40	1.29	1.47

TABLE IV
MAXIMUM HEIGHT ERROR FOR DIFFERENT PEDESTRIANS

max.err. [m]	60-75 kg	76-90 kg
age 20-30	3.72	3.55
age 31-40	3.46	4.22

TABLE V
FOOT STEP DETECTION COMPARISON BETWEEN ADAPTIVE ZUPT METHOD AND POSITIVE ZERO-CROSSING METHOD

number of foot step	walking	running
positive zero-crossing	291	203
adaptive ZUPT	291	201
detection correctness (%)	100	99

during the experiments. The experimental setup is the same as in Fig. 16. As can been seen that the maximum error variations for both errors are less than 1 m. However, we do find out that the irregular walking/running poses can affect the tracking accuracy. This issue will be investigated in the future study.

Nevertheless, the adaptive ZUPT algorithm does remove significant amount of accumulative error. One is still able to recover the actual trajectory and differentiate the walking at the same floor from stairs climbing.

Afterwards the resulted trajectories using conventional ZUPT method will be compared with our results. 2 possibilities have been considered. One is to choose a pre-defined ZUPT threshold value so that the still-phases at walking speed can be successfully detected. This value should be very close to $\delta_{\mathrm{ZUPT},1}$ as plotted in Fig. 5. Since $\delta_{\mathrm{ZUPT},1}$ is too small for the still-phases detection at running speed and the accumulative velocity error can not be removed, the obtained position updates within this time duration are much larger than the actual ones. The other possibility is to choose a bigger threshold value such as $\delta_{\mathrm{ZUPT},2}$ given in Fig. 5 so that the still-phases during the time of running can be detected. However, in this way, $\delta_{\mathrm{ZUPT},2}$ is big enough to also reset the velocity during the swing-phases to zero at walking speed. Therefore, the obtained position updates within this time duration is much smaller than the actual one. The tracking trajectories using conventional ZUPT and adaptive ZUPT methods are depicted in Fig. 24 and 25.

In order to evaluate the performance consistence of proposed adaptive ZUPT method, the same experiment has been repeated for 10 times. The number of foot steps detected by adaptive ZUPT method is compared with the misdetection-free step number using positive zero-crossing method. As a result, adaptive ZUPT method is able to detect all the still-phases during walking phase and achieve a 99% correctness of the still-phase detection during running phase, as given in Table. V.

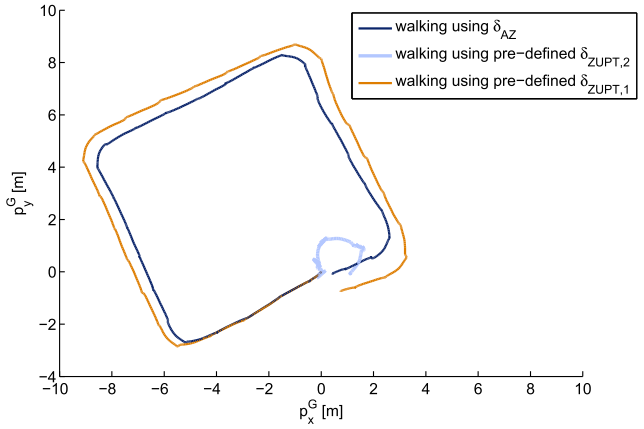

Fig. 24. Comparison of resulted 2D trajectories during walking phase using adaptive and conventional ZUPT methods.

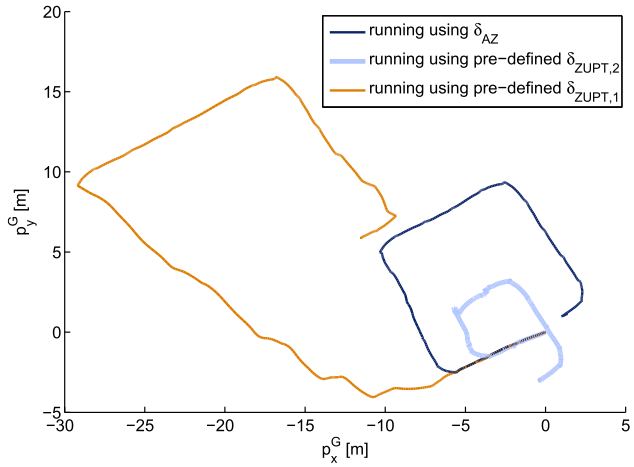

Fig. 25. Comparison of resulted 2D trajectories during running phase using adaptive and conventional ZUPT methods.

VI. Conclusion

This paper presents an adaptive ZUPT approach which requires an additional acceleration sensor to detect the still-phases when the velocity is changing. The information extracted from the chest acceleration is used to determine the speed-dependent threshold for detecting the still-phase. Instead of using the complex wavelet transform in our previous work, this study uses the maximum acceleration change during each foot step to differentiate the movements at different speeds, which is more computation- and energy-friendly especially for hardware programming and implementation. Furthermore, unlike the empirical transition model obtained in our previous work, a treadmill experiment has been carried out to determine the relation between the maximum acceleration change during each foot step and ZUPT threshold. 9 different speeds from 5 km/h to 18 km/h are investigated to enhance the reliability of relation model. The foot-mounted IMU module is used to track the pedestrian using the navigation algorithm which utilizes the appropriate threshold to detect the still-phases at different speeds.

An experiment has been carried out to evaluate the performance of proposed adaptive ZUPT method. Fig. 18 shows that the maximum acceleration change during each foot step correctly indicates the change of speed. By applying the relation model between the maximum acceleration change during each foot step and threshold given by Fig. 14, the thresholds which are corresponding to the speed changes during the experiment can be determined as shown in Fig. 19. As a result, the still-phases of each step during the experiment have been successfully detected as depicted in Fig. 20, which is followed by accumulative-error-free velocities and positions as depicted in Fig. 21 and 22. In comparison with the result achieved by conventional ZUPT as depicted in Fig. 24 and 25, the proposed adaptive ZUPT approach brings a significant improvement.

Although adaptive ZUPT method is able to expand the usage of conventional ZUPT for walking-like movements with changing speed, how to remove accumulative error of non-walking-like movements such as climbing, jumping and creeping are still left to be studied. Cooperation with people from the research fields of kinematic models and bio-mechanic might be helpful to find the different sort of 'still-phase' for irregular movements to minimize the sensor error.

Acknowledgment

The authors would like to thank C. Heyde for accomplishing the treadmill experiment and providing the relevant equipments.

References

[1] C. Fischer and H. Gellersen, "Location and navigation support for emergency responders: A survey," *Pervasive Comput.*, vol. 9, no. 1, pp. 38–47, Jan./Mar. 2010.

[2] K. N. Vikas, "Integration of inertial navigation system and global positioning system using Kalman filtering," Ph.D. dissertation, Dept. Aerosp. Eng., Indian Inst. Technol., Bombay, India, 2004.

[3] L. Ojeda and J. Borenstein, "Non-GPS navigation for security personnel and first responders," *J. Navigat.*, vol. 60, no. 3, pp. 391–407, 2007.

[4] L. Ojeda and J. Borenstein, "Personal dead-reckoning system for GPS-denied environments," in *Proc. IEEE SSRR*, Sep. 2007, pp. 1–6.

[5] E. Foxlin, "Pedestrian tracking with shoe-mounted inertial sensors," *IEEE Comput. Graph. Appl.*, vol. 25, no. 6, pp. 38–46, Nov./Dec. 2005.

[6] S. Y. Cho and C. G. Park, "MEMS based pedestrian navigation system," *J. Navigat.*, vol. 59, no. 1, pp. 135–153, 2006.

[7] A. R. Jiménez, F. Seco, J. C. Prieto, and J. Guevara, "Indoor pedestrian navigation using an INS/EKF framework for yaw drift reduction and a foot-mounted IMU," in *Proc. 7th Workshop Position. Navigat. Commun. (WPNC)*, Mar. 2010, pp. 135–143.

[8] A. R. Jiménez, F. Seco, J. C. Prieto, and J. Guevara, "Accurate pedestrian indoor navigation by tightly coupling foot-mounted IMU and RFID measurements," *IEEE Trans. Instrum. Meas.*, vol. 61, no. 1, pp. 178–189, Jan. 2012.

[9] J. Calusdian, X. Yun, and E. R. Bachmann, "Adaptive-gain complementary filter of inertial and magnetic data for orientation estimation," in *Proc. IEEE Int. Conf. Robot. Autom. (ICRA)*, May 2011, pp. 1916–1922.

[10] X. Yun, J. Calusdian, E. R. Bachmann, and R. B. McGhee, "Estimation of human foot motion during normal walking using inertial and magnetic sensor measurements," *IEEE Trans. Instrum. Meas.*, vol. 61, no. 7, pp. 2059–2072, Jul. 2012.

[11] F. Höeflinger, J. Müeller, R. Zhang, L. M. Reindl, and W. Burgard, "A wireless micro inertial measurement unit (IMU)," *IEEE Trans. Instrum. Meas.*, vol. 62, no. 8, pp. 2583–2595, Sep. 2013.

[12] R. Zhang, F. Hoeflinger, and L. M. Reindl, "Inertial sensor based indoor localization and monitoring system for emergency responders," *IEEE Sensors J.*, vol. 13, no. 2, pp. 838–848, Feb. 2013.

[13] R. Feliz, E. Zalama, and J. G. García-Bermejo, "Pedestrian tracking using inertial sensors," *J. Phys. Agents*, vol. 3, no. 1, Jan. 2009.

[14] R. Zhang, M. Loschonsky, and L. M. Reindl, "Study of zero velocity update for both Low- and high-speed human activities," *Int. J. E-Health Med. Commun.*, vol. 2, no. 2, pp. 46–67, 2011.

[15] N. Ravi, N. Dandekar, P. Mysore, and M. L. Littman, "Activity recognition from accelerometer data," in *Proc. 17th Conf. Innov. Appl. Artif. Intell.*, 2005, pp. 1541–1546.

[16] M. Sekine, T. Tamura, M. Ogawa, T. Togawa, and Y. Fukui, "Classification of acceleration waveform in a continuous walking record," in *Proc. IEEE IEMBS*, vol. 3, Nov. 1998, pp. 1523–1526.

[17] M. Sekine, T. Tamura, M. Fujimoto, and Y. Fukui, "Classification of walking pattern using acceleration waveform in elderly people," in *Proc. 22nd Annu. EMBS Int. Conf.*, vol. 2, Jul. 2000, pp. 1356–1359.

[18] M. Sekine, T. Tamura, T. Akay, M. Fujimoto, T. Togawa, and Y. Fukui, "Discrimination of walking patterns using wavelet-based fractal analysis," *IEEE Trans. Neural Syst. Rehabil. Eng.*, vol. 10, no. 3, pp. 188–196, Sep. 2002.

[19] M. J. Mathie, B. G. Celler, N. H. Lovell, and A. C. F. Coster, "Classification of basic daily movements using a triaxial accelerometer," *Med. Biol. Eng. Comput.*, vol. 42, no. 5, pp. 679–687, 2004.

[20] B. Najafi, K. Aminian, A. Paraschiv-Ionescu, F. Loew, C. J. Büla, and P. Robert, "Ambulatory system for human motion analysis using a kinematic sensor: Monitoring of daily physical activity in the elderly," *IEEE Trans. Biomed. Eng.*, vol. 50, no. 6, pp. 711–723, Jun. 2003.

[21] S. Beauregard and H. Haas, "Pedestrian dead reckoning: A basis for personal positioning," in *Proc. WPNC*, 2006, pp. 27–35.

[22] *Xsens. MTx*. [Online]. Available: https://www.xsens.com/products/mtx/

Rui Zhang received the B.Sc. degree from the Beijing University of Aeronautics and Astronautics, Beijing, China, and the M.Sc. degree from the Institute of Telecommunications, Darmstadt University of Technology, Darmstadt, Germany, in 2006 and 2009, respectively, and the Ph.D. degree from the Laboratory for Electrical Instrumentation, Institute of Microsystem Technology, University of Freiburg, Germany, in 2014. He was a recipient of the Siemens Master Program Scholarship for the Master study in Germany in 2006.

He currently holds a Post-Doctoral position with the University of Freiburg. His current research interests include inertial sensor-based and wireless infrastructure-based localization, inertial sensor-based applications, and data processing such as movement monitoring and physical parameter extraction.

Hai Yang was born in 1988. He received the B.E. and M.E. degrees from the School of Mechatronic Engineering, China University of Mining and Technology, Xuzhou, China, in 2011 and 2013, respectively, where he is currently pursuing the Ph.D. degree. His research interests include inertial navigation system and integrated positioning system.

Fabian Höflinger received the B.Sc. degree in automation engineering from the University of Applied Sciences, Ravensburg, and the master's degree in automation and energy systems from the University of Applied Sciences, Mannheim, in 2007, where he developed inductive electronic components. From 2007 to 2010, he was employed as a Development Engineer. He was with Junghans Feinwerktechnik, where he developed components for telemetric systems. He received the Ph.D. degree in localization systems for determining the position of people and objects in indoor areas in 2014. Since 2010, he has been with the Laboratory for Electrical Instrumentation, Department of Microsystems Engineering, University of Freiburg. Since 2014, he has been Group Leader and is building up a research group in the field of indoor-localization.

Leonhard M. Reindl received the Diploma degree in physics from the Technische Universität München, Munich, Germany, and the Dr.Sc.techn. degree from the Vienna University of Technology, Vienna, Austria, in 1985 and 1997, respectively. He joined the Surface Acoustic Wave Department, Siemens Corporate Technology Division, Munich, Germany, in 1985, where he was engaged in the development of surface acoustic wave (SAW) devices for signal processing and matched filtering in radio communications, radar systems, SAW-based identification marks, and wireless passive SAW-based sensors. In 1999, he joined the Institute of Electrical Information Technology, Clausthal University of Technology, Clausthal-Zellerfeld, Germany. In 2003, he joined as a Full Professor of Electrical Instrumentation the Institute for Microsystem Technology, Albert-Ludwigs University of Freiburg, Freiburg, Germany. He has authored or co-authored over 250 papers on SAW devices and wireless passive sensor systems and holds 45 patents. His current research interests include wireless sensor systems, energy-harvesting systems, local positioning systems, and search and rescue systems for people buried in disasters.

Dr. Reindl is a member of the Technical Program Committees of the IEEE Frequency Control Symposium, the IEEE Ultrasonic Symposium, Eurosensors, Sensors, and the German Biannual Symposium Sensoren und Messsysteme. He was an Elected Member of the AdCom of the IEEE UFFC Society from 2005 to 2007 and from 2010 to 2012.